

A Fast Multi-focus Image Fusion Algorithm by DWT and Focused Region Decision Map

Shumin Liu and Jiajia Chen

E-mail: shumin_liu@mymail.sutd.edu.sg; jiajia_chen@sutd.edu.sg
Singapore University of Technology and Design, Singapore

Abstract—To comprise the advantages of both the spatial domain and transform domain methods, this paper presents a novel hybrid algorithm for multi-focus images fusion, which reduces the error rate of sub-band coefficients selection in the transform domain and reduce the artificial discontinuities created in the spatial domain algorithms. In this method, wavelet transforms are firstly performed on each input image, and a focused region decision map is established based on the high-frequency sub-bands extraction. The fusion rules are then guided by this map, and the fused coefficients are transformed back to form the fused image. Experimental results demonstrate that the proposed method is better than various existing methods, in term of fusion quality benchmarks. In addition, the proposed algorithm has a complexity proportional to the total number of pixels in the image, which is lower than some other algorithm which may produce similar fusion quality with the proposed algorithm. Furthermore, the proposed algorithm only requires one level wavelet decomposition, again reducing the processing time. With the proposed method, high quality and fast multi-focus image fusion is made possible.

I. INTRODUCTION

Due to the limitation of optical technology, a single image can only present information with a single depth-of-focus [1]. The objects which are not at the depth-of-focus appeared out of focus in the image and hence not displayed sharply. Motivated by the effective image processing and applications in military surveillance, meteorological phenomena and biomedical cells monitoring, multiple images can be captured for the same scene with different depth-of-focus, and dedicated multi-focus image fusion methods can be applied to produce a fused image with multiple objects focused.

Image fusion is a process of combining complementary information from multiple images of the same scene into an image containing more information of the scene. The multi-focus image fusion methods can be generally categorized into spatial domain or transform domain [2]. In the spatial domain approaches, images are fused directly from the input images with a set of fusion rules. An important type of spatial method is called the focused region method [3], and its fundamental is the selection of sharper images regions from the input images and directly copy the pixels into the fused image [4]. This method is usually shift-invariant and only affected limitedly by mis-registration of input images. However, this method may generate artificial information and discontinuity at the boundary when the focused region decision map is not determined accurately. The transform domain approach, on

the other hand, transforms the input images into a series of sub-images. The fusion rules are then applied on these sub-images and the final fused image is obtained by a corresponding inverse transform. This category includes the Gradient Pyramid Transform (GPT) [5], Discrete Wavelet Transform (DWT) [6], and Nonsubsampled Contourlet Transform (NSCT) [7]. With these transformations, high and low-frequency sub-bands can be effectively separated and the fusion rules are made based on these information. However, all transform methods suffers from the loss of information due to the imperfections of the fusion rules.

Because of the unavoidable errors by the focused region methods and the transform methods, the proposed hybrid method in this paper combines these two approaches by applying the focused region method for regions which are probably to be focused in any of the input images and the transform method for the regions that are indecisive. With this hybrid approach, the misselection of coefficients in the transform domain can be significantly reduced with limited discontinuities created. In addition, the proposed algorithm also aims at the reduced computational complexity over the existing approaches, owing to the larger image and video resolution under processing. From the experiments, it has been shown that the proposed method utilizing wavelet transform is capable to produce high quality multi-focus image within a shorter processing time.

II. PRELIMINARIES OF 2D DISCRETE WAVELET TRANSFORM AND PROPOSED ALGORITHM OVERVIEW

A L -level 2-dimensional DWT on an image will produce $(3L+1)$ sub-bands, where one of them contains the low-frequency information, and $3L$ of them contains the high-frequency information for each level in the horizontal, vertical and diagonal directions [8]. For the proposed algorithm, one level DWT would be sufficient because the first level coefficients contain information with the highest frequency, which are critical for the fusion rules and the focused region decision map.

Another critical factor for the rules and map is the completeness of information, in other words, the shift invariance of the transform. The popular wavelet transforms which aim for improved shift invariance include complex DWT (CDWT) [9] and undecimated DWT [10]. At the level one decomposition, they have the same redundancy. For the

proposed algorithm, CDWT is used as it has more freedom on the redundancy, thus a better balance between shift invariance and processing time. The concept of CDWT is only used in the decomposition steps for the decision map, original DWT is used in the reconstruction steps for reduced processing time.

A very popular and simple fusion rule for the high-frequency sub-bands is the selection of coefficients which have the largest absolute value [8]. Furthermore, if most coefficients are selected from a specified region of the same image, it is almost certain that the image is focused at that region. As a result, a focused region decision map can be generated from the high-frequency sub-bands, and it has two types of regions: regions with a confirmed focused image and regions that are indecisive. Therefore, the proposed algorithm flowchart is shown in Fig. 1 below, whose details will be presented in Section III.

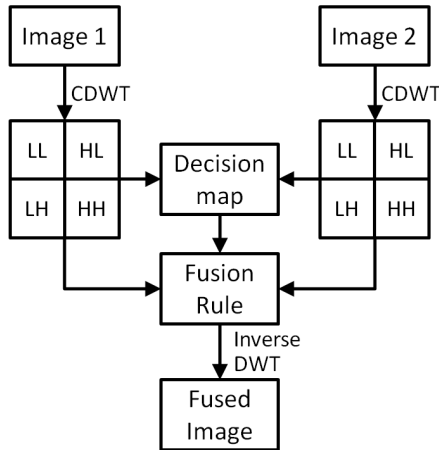


Fig. 1 Overall flowchart of the proposed image fusion algorithm.

III. THE PROPOSED ALGORITHM

In this section, a multi-focus fusion algorithm on two monochrome images I_1 and I_2 , each with size $N \times M$ will be presented, where N and M are assumed to be even. Haar filter will be used as it is the simplest wavelet filter and it is effective in separating the high and low frequency sub-bands [11].

A. The sub-band extraction

For two dimensional CDWT, the redundancy factor is 4 [9], this is done by delaying the signal in horizontal, vertical and diagonal directions. However, it can be seen in Fig. 2 that not all redundancy is needed by the decision map. If an image starts with pixel a , the differences between a, b, d and e will be registered by the original DWT, and the differences between e, f, h and i will be registered by CDWT delaying in the diagonal direction. These two sets of DWT are able to register all the edges in an image with a redundancy factor of 2.

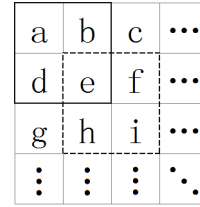


Fig. 2 The level one high-frequency CDWT.

The output of CDWT performed would be $D_1^l, D_1^h, D_1^v, D_1^d, D_2^l, D_2^h, D_2^v, D_2^d$ and $E_1^l, E_1^h, E_1^v, E_1^d, E_2^l, E_2^h, E_2^v, E_2^d$. D represents wavelet coefficients generated from non-delayed image, whereas E represents that from image with outmost pixels removed. The superscripts l, h, v and d represent low-frequency, horizontal, vertical and diagonal high-frequency sub-bands respectively. The subscripts 1 and 2 indicate which image does this sub-band generated from.

To evaluate the information over all the high-frequency sub-bands, the three high-frequency sub-bands from D and E are firstly combined to derive the combined sub-bands, D_i^c, E_i^c , as shown in (1) where $i = 1$ or 2 .

$$\begin{aligned} D_i^c &= (D_i^h)^2 + (D_i^v)^2 + (D_i^d)^2 \\ E_i^c &= (E_i^h)^2 + (E_i^v)^2 + (E_i^d)^2 \end{aligned} \quad (1)$$

To effectively determine the sharpness for the calculations in the next step, D^c and E^c of each image are then merged to develop a comprehensive high-frequency sub-bands, H . However, images with the outmost pixels removed have a size of $(N-2) \times (M-2)$, thus its wavelet sub-bands, E , have a size of $(N/2-1) \times (M/2-1)$. As the size of D is $(N/2) \times (M/2)$, a convolution of E should be performed with $[0.25 \ 0.25; 0.25 \ 0.25]$ to match the size and position of D . The elements of the matrix sum up to 1, which means D and E have the same weightage when producing H , as shown in (2) where $i = 1$ or 2 .

$$H_i = D_i^c + E_i^c * \begin{bmatrix} 0.25 & 0.25 \\ 0.25 & 0.25 \end{bmatrix} \quad (2)$$

As errors are more prone to occur at the border of an image, the outmost coefficients of H are set to zero to reduce the error.

B. The decision map

After H_i for each image is computed, the next step is to construct a decision map. First of all, a square window with an odd number of rows/columns is used to ensure that the averaging effect is centered at the target pixel, and the effects are the same in the horizontal and vertical directions. The size of the window is a variable which should be carefully selected based on the image resolution. An overly sized window would cause the decision map to lose details at the borders between focused and non-focused regions, while an insufficiently sized window cannot contribute an effective denoising. As most of the images employed for experiment in this paper have size from 256 to 640, the window size is selected as 7 by trial evaluation, as shown in Fig. 3. Only elements occupied by a circle of diameter 7 centered in the middle of the window will

be given the value of one; otherwise, the values are set to zero. Comparing with the window with all ones, this window is more correlated with the distance from the center and hence can perform better averaging in the images with less calculation time. After setting up the window, the difference between H_1, H_2 for each pixel is denoised by the 7×7 window w , and the output is defined as δ as shown in (3). For the rest of the paper, it is assumed that for convolutions from an input and a window, the output has the same size as the input by only taking the center coefficients.

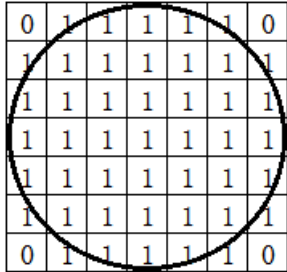


Fig. 3 The 7×7 window proposed.

$$\delta = (H_1 - H_2) * w \quad (3)$$

From (3), δ provides the information on which image a pixel is more focused. A pixel is more focused in image 1 if δ is positive, and more focused in image 2 if δ is negative. The difference is indecisive if δ is zero. As described in Section II, the image is very likely focused at a region if most pixels at that region of the image are more focused than the other image. The weight function, W , is needed to analyze the ownership of a region around a pixel to decide its focus zone as in (4). The same 7×7 window is used in this process for the same reason described earlier. By convoluting the sign of δ with this window, W denotes the difference between the numbers of pixels belongs to image 1 and that of image 2. If the difference is more than half of the window size, the pixel is decisive; else it is indecisive. This generates the final ownership of the pixels, and this information will be stored in the proposed focused region decision map, M in (5) where (x, y) stand for the position of coefficients in the level one wavelet sub-bands. For the threshold, a large threshold value would result in a wider indecisive region where a small threshold would result in more wrongly decided pixels. In our algorithm, therefore, we choose it to be 22.5, which is half the sum of elements in w .

$$W = \text{sign}(\delta) * w \quad (4)$$

$$M(x, y) = \begin{cases} 1 & \text{if } W(x, y) > 22.5 \\ 2 & \text{if } W(x, y) < -22.5 \\ 0 & \text{else} \end{cases} \quad (5)$$

C. The fusion rules

During the fusion of two images I_1 and I_2 , the decision map can have three different values which are 0, 1 and 2, so there are three sets of fusion rules proposed in our algorithm. If a pixel belongs to I_1 , the fused sub-bands, Y , will copy the DWT coefficients from the sub-bands of I_1 . The same rule is applied for pixels belong to I_2 , as shown in (6).

$$Y(x, y) = \begin{cases} D_1(x, y) & \text{if } Map(x, y) = 1 \\ D_2(x, y) & \text{if } Map(x, y) = 2 \end{cases} \quad (6)$$

For pixels that are indecisive, a linearly weighted summation of low-frequency sub-bands will be performed based on the value of W . The value of W is ranged from -22.5 to 22.5 , and this can be rescaled to a function $k(x, y)$ which ranges from 0 to 1, as shown in (7) to (9). This will create a smooth transition in the indecisive regions, reducing the amount of artificial information created.

$$Y^l(x, y) = U^l(x, y) \quad \text{if } Map(x, y) = 0 \quad (7)$$

$$k(x, y) = [22.5 - W(x, y)] / 45 \quad (8)$$

$$U^l(x, y) = (1 - k) \times D_1^l + k \times D_2^l \quad (9)$$

For the high-frequency sub-bands, the largest absolute value rule is applied. The fusion rule for high-frequency sub-bands in the horizontal direction is shown in (10) and (11), and this rule is exactly the same in the vertical and diagonal directions.

$$Y^h(x, y) = U^h(x, y) \quad \text{if } Map(x, y) = 0 \quad (10)$$

$$U^h(x, y) = \begin{cases} D_1^h & \text{if } |D_1^h| > |D_2^h| \\ D_2^h & \text{else} \end{cases} \quad (11)$$

The fused image, F , can be obtained by inverse DWT of Y .

IV. EXPERIMENT RESULTS AND DISCUSSIONS

In this section, the quality of fused images by the proposed method will be prudently evaluated. The algorithm computational complexity and CPU time will be evaluated too. The proposed algorithm is compared with a group of relevant competing methods, including Gradient Pyramid Transform (GPT) [5], Discrete Wavelet Transform [8], Nonsubsampled Contourlet Transforms: NSCT1 [12] and NSCT2 [3], a bilateral gradient-based sharpness based (BGBS) [13] and a Hybrid method [3]. The first 4 methods, GPT, DWT, NSCT1 and NSCT2 are in the transform domain. BGBS is the method in the spatial domain, and Hybrid is a hybrid of transform and spatial domain methods with the last step using the focused region method. We have modeled all these competing algorithms following exactly the proposed steps in their respective papers, where the ‘averaging’ rule is used in the low-frequency sub-band to replace the contrast increasing rule proposed in GPT. ‘Haar’ filter is used in DWT and four level decomposition with 1, 2, 4 and 8 directions is used in NSCT1 and NSCT2, with ‘maxflat’ as the pyramidal filter and ‘dmaxflat7’ as the directional filter [14].

A. The effectiveness of complex wavelet decomposition

Benchmark images are employed to evaluate the effectiveness of the proposed algorithm. A 4-times difference images (DI), between the fused and input images are used [15] as it can clearly point out the magnitude and position of the defects in the fused image. The formula of DI is shown in (10), where F is the fused image and I_i are the input images with $i = 1$ or 2.

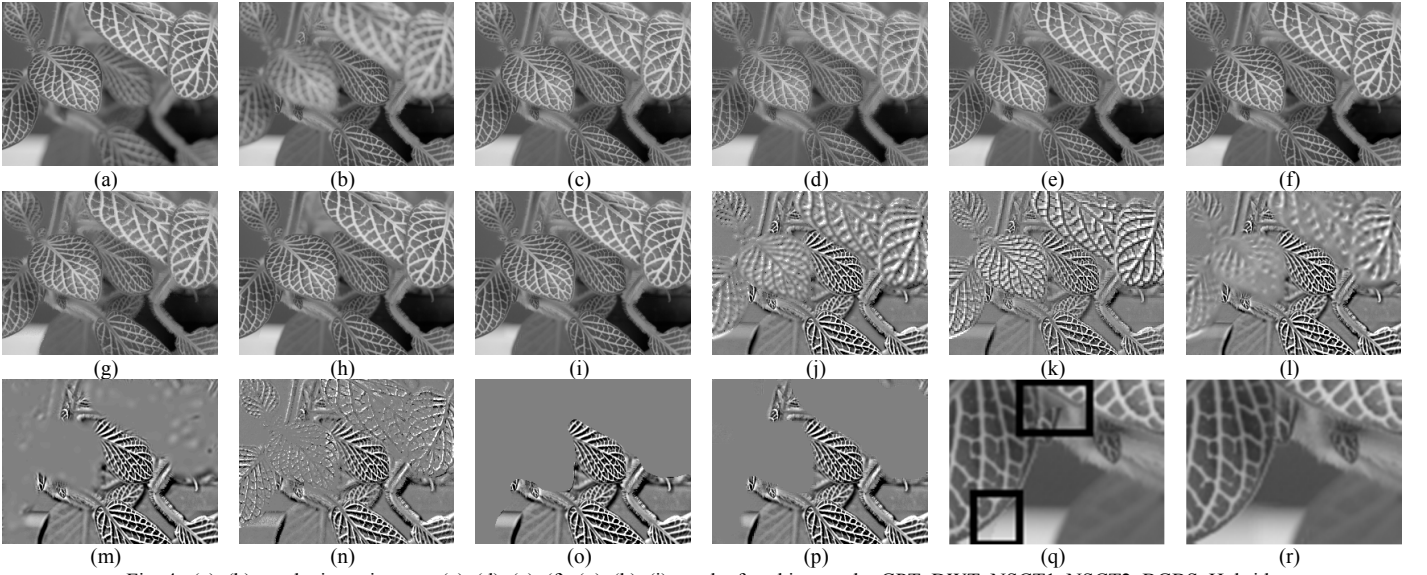


Fig. 4 (a), (b) are the input images; (c), (d), (e), (f), (g), (h), (i) are the fused images by GPT, DWT, NSCT1, NSCT2, BGBS, Hybrid and proposed method respectively; (j), (k), (l), (m), (n), (o), (p) the respective DI1; (q), (r) are the bottom left zoom in images for (h), (i).

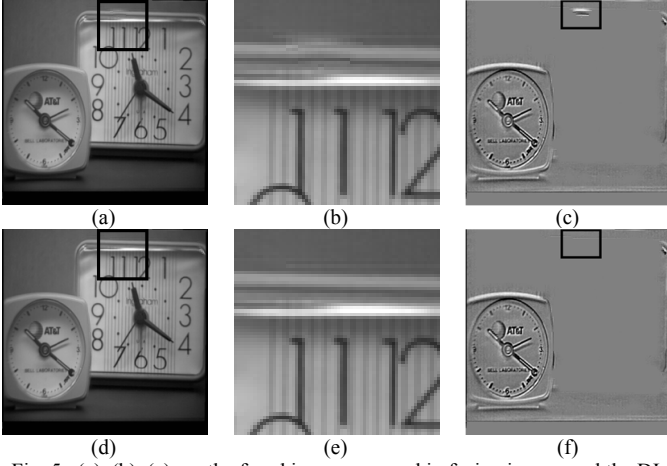


Fig. 5 (a), (b), (c) are the fused image, zoomed in fusion image, and the DI for input 2 using original DWT; (d), (e), (f) are the fused image, zoomed in fusion image, and DI2 using the proposed CDWT.

$$DI_i = (F - I_i) \times 4 + 127.5 \quad (12)$$

From Fig. 5, it can be clearly seen that an error occurs at the top of the fused image without using CDWT in the decomposition steps. This error causes some discontinuity in the fused image shown in (b) and some strong noises on the DI shown in (c) highlighted by the black box. This effect due to the incomplete high-frequency decomposition adds some artificial information and removes some useful information in the fused image.

B. Comparison of the fused images for fusion discontinuities and errors

From Fig. 4, it can be seen clearly that Hybrid produces the best DI among the seven methods. It has absolutely no noise in areas that are far away from the boundary of focused and non-focused regions. Our proposed method produced the second best DI, as the noise is only at limited regions with






limited magnitude. NSCT2 produces slightly worse DI than the proposed and all other methods produce unsatisfactory DI.

Although Hybrid embraces the advantages from both the spatial and transform domain, it is unable to solve the problem existing in the focused region method. As shown in Fig. 4 (q), there are two clear discontinuities at the bottom left corner and this greatly reduces the quality of the fused image. Moreover, at the top of the image, the hybrid method misidentifies a far-focused region as a near-focused region and hence copies the pixel values from the wrong input image as in Fig 4(o). On the other hand, Fig. 5 (r) and (p) by the proposed method does not possess such problems, as it does not use the focused region method in the last step. It can also be seen that the GPT, DWT and NSCT1 possess considerable errors from misregistration. For example, the boundary of leaf and the background is not clear at the bottom left corner for the three methods as in (c), (d) and (e). From the above analysis, it can be concluded that the proposed method is the best among the seven methods in term of discontinuities and errors in the fused images.

C. 2-input image fusion and comparison using benchmarks

Five pairs of images are employed in this section to compare the fused image quality by the competing methods and the proposed algorithm. Each pair includes images of the same object with two different focused points. The three benchmarks, average gradient (AG) [16], edge dependent fusion quality index (Q_E) [17] and edge based similarity measure ($Q^{I/F}$) [18] are used. They are all gradient or edge based benchmarks because the clarity of edge is very important for multi-focus image fusion. It can be shown in Table I that the overall benchmark evaluations for Hybrid and the proposed method are similar and the best two among the seven methods. Furthermore, the ratios between the scores by the proposed algorithm and the best score for the same image are always larger than 99.5% for all benchmarks. The good quality of the proposed method comes from its hybrid features

TABLE I
BENCHMARKS FOR IMAGES WITHOUT A PERFECT FUSED IMAGE

Image	Benchmark	GPT	DWT	NSCT1	NSCT2	BGBS	Hybrid	Proposed
	AG	6.4651	5.8871	6.4521	6.6347	6.0406	6.5979	6.6754
	Q_E	0.88502	0.8672	0.89273	0.89744	0.87327	0.89289	0.89398
	$Q^{I/F}$	0.8436	0.81636	0.85273	0.87512	0.82168	0.8877	0.88666
	AG	4.1528	3.5708	4.3986	4.446	4.3233	4.3903	4.462
	Q_E	0.89989	0.87111	0.90447	0.91249	0.89349	0.91305	0.91407
	$Q^{I/F}$	0.83265	0.79134	0.85881	0.8835	0.82573	0.89864	0.89598
	AG	12.6997	11.3099	12.8445	13.1838	12.0415	13.1051	13.2744
	Q_E	0.83177	0.77344	0.84723	0.85767	0.81327	0.8538	0.85837
	$Q^{I/F}$	0.84464	0.79685	0.85854	0.88632	0.82874	0.89396	0.89421
	AG	5.5842	5.1821	5.635	5.6377	5.1396	5.6265	5.7124
	Q_E	0.94413	0.89643	0.9481	0.94978	0.9283	0.9506	0.9506
	$Q^{I/F}$	0.87123	0.84352	0.87963	0.89357	0.84162	0.90153	0.89883
	AG	7.3609	6.737	7.5571	7.7628	7.2471	7.762	7.8014
	Q_E	0.88725	0.88225	0.88653	0.88901	0.88991	0.88717	0.8885
	$Q^{I/F}$	0.8268	0.80312	0.84098	0.86241	0.80833	0.87369	0.87317

with the focused region method, and this can be shown by the comparison with the sole DWT. Although Hybrid can produce similar quality, its good quality comes from its higher computational complexity, and this can be shown in Part E of this session.

D. Fusion with more than 2 color images

The proposed algorithm can be easily extended to colored images. For the combined coefficients in equation (1), it is the sum of the squared values for 3 high-frequency sub-bands. In a colored image, there are usually 3 layers and thus 9 high-frequency sub-bands in total for level one wavelet decomposition. The only changes needed are D and E from the sum square of three values to nine values as shown in (11), where $i = 1$ or 2 indicating the input image number, and R,G,B stand for the red, green and blue layer of a colored image.

$$\begin{aligned} D_i^c &= (D_{i,R}^c)^2 + (D_{i,G}^c)^2 + (D_{i,B}^c)^2 \\ E_i^c &= (E_{i,R}^c)^2 + (E_{i,G}^c)^2 + (E_{i,B}^c)^2 \end{aligned} \quad (13)$$

There are 2 ways to apply the proposed algorithm to multiple images fusion. A simpler one would be using exactly the same algorithm to fuse the images in a binary tree structure, thus L number of images require $L-1$ fusions.

A more comprehensive way for multiple images fusion requires the modification of algorithm from (3). The data structure of W in (4) should be changed from a $N \times M$ array to L numbers of $N \times M$ arrays, each array records the numbers of pixels belongs to image i in a 7×7 windows as shown in (12), (13) and (14), where $i \in L$.

$$G_i = H_i * w \quad (14)$$

$$f_i(x, y) = \begin{cases} 1 & \text{if } G_i(x, y) = \max_{l \in L} G_l(x, y) \\ 0 & \text{else} \end{cases} \quad (15)$$

$$W_i = f_i * w \quad (16)$$

After W , the decision map and low-frequency fusion rule for the indecisive pixels should be modified accordingly, whereas all other steps remain unchanged. The concept behind generating Map is identical to that of 2-inputs algorithm: a pixel belongs to image i if there are 22.5 more pixels belongs to image i comparing with the rest, as shown in (15).

$$Map(x, y) = \begin{cases} 1 & \text{if } W_1 - \sum_{i \in L, i \neq 1} W_i > 22.5 \\ 2 & \text{if } W_2 - \sum_{i \in L, i \neq 2} W_i > 22.5 \\ \dots & \\ 0 & \text{else} \end{cases} \quad (17)$$

For the low-frequency sub-bands in the indecisive region, quadratic ratio on W is used to generate the fused low-frequency coefficients as shown in (16) and (17). Just as the 2-inputs algorithm, this steps aim to create a smooth transition in the indecisive regions and reduce the amount of artificial information created. The testing image for 3-inputs color fusion in Fig. 6 shows good fused image quality.

$$k_i(x, y) = \frac{W_i(x, y)^2}{\sum_{l \in L} W_l(x, y)^2} \quad (18)$$

$$U^l(x, y) = \sum_{l \in L} k_l(x, y) \times D_l^l(x, y) \quad (19)$$

TABLE II
THE COMPLEXITY AND PROCESSING TIME

Method	Computational Complexity	256×256		480×640	
		CPU Time /s	Real Time /s	CPU Time /s	Real Time /s
GPT	$N \times M$	0.0133	0.0068	0.0417	0.0170
DWT	$N \times M$	0.0159	0.0103	0.0950	0.0613
NSCT1	$N \times M$	85.4729	85.4008	404.1830	403.8878
NSCT2	$(N \times M)^2$	26.1614	18.5748	139.9953	111.1095
BGBS	$N \times M$	0.0129	0.0079	0.0604	0.0300
Hybrid	$(N \times M)^2$	28.4858	19.9742	141.7581	112.6296
Proposed	$N \times M$	0.0254	0.0168	0.1596	0.1001

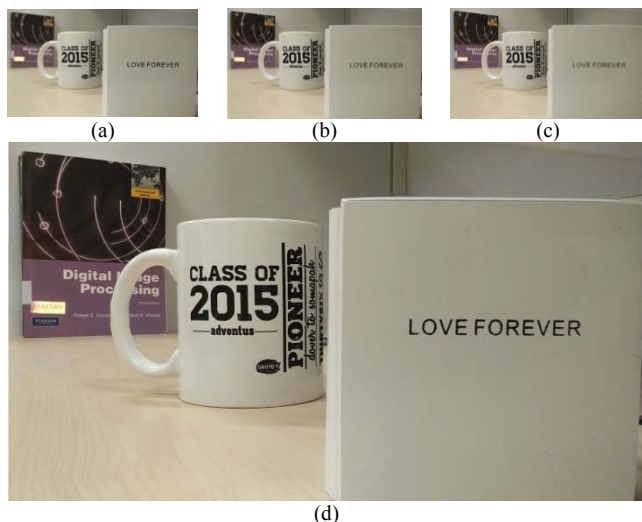


Fig. 6 An example of a 3-inputs color fused image: (a), (b), (c) the input images focused at the note, cup and book respectively; (d) the fused image.

E. The algorithm complexity and processing time

All the experiments to fuse 256×256 and 480×640 images are performed using MATLAB R2013b on the same platform with i7-4810MQ CPU at 2.8GHz and 16 GB RAM. It can be clearly seen in Table II that except NSCT2 and hybrid methods, all other methods have the same complexity as $N \times M$. Although the proposed method is the second slowest in terms of CPU time among these five algorithms with complexity $N \times M$, this computation effort is worthy as it significantly improved the quality of the fused image without a significant increase in the CPU time. For Hybrid and the proposed algorithm which produce the similar fused image quality, the proposed method has a much lower complexity at $N \times M$ compared with $(N \times M)^2$ by Hybrid. The CPU time has been saved significantly by the proposed algorithm too, up to a thousand times over Hybrid algorithm.

V. CONCLUSION

In this paper, a novel image fusion method using the hybrid of DWT and the focused area decision map is proposed for multi-focus image fusion. The experimental results demonstrate that the proposed method is able to produce high quality fused image with lower algorithm complexity. In the future work, parallelism will be considered to accelerate the

algorithm to satisfy the requirements for high-definition real-time applications.

ACKNOWLEDGMENT

In this paper, the NSCT toolboxes from Arthur Cunha (<http://www.mathworks.com/matlabcentral/fileexchange/10049-nonsubsampled-contourlet-toolbox>) is adopted for the testing process. His share is deeply appreciated.

REFERENCES

- [1] S. Li, and B. Yang, "Multifocus image fusion using region segmentation and spatial frequency," *Image and Vision Computing*, vol. 26, no. 7, pp. 971-979, Jul. 2008.
- [2] N. Mitianoudis, and T. Stathaki, "Optimal contrast correction for ICA-based fusion of multimodal images," *IEEE Trans. on Sensors Journal*, vol. 8, no. 12, pp. 2016-2026, Dec. 2008.
- [3] Y. Yang, S. Tong, S. Huang *et al.*, "Multifocus image fusion based on NSCT and focused area detection," *IEEE Trans. on Sensors Journal*, vol. 15, no. 5, pp. 2824-2838, May 2015.
- [4] V. Aslantas, and R. Kurban, "Fusion of multi-focus images using differential evolution algorithm," *Expert Systems with Applications*, vol. 37, no. 12, pp. 8861-8870, Dec. 2010.
- [5] V. S. Petrović, and C. S. Xydeas, "Gradient-based multiresolution image fusion," *IEEE Trans. on Image Processing*, vol. 13, no. 2, pp. 228-237, Feb. 2004.
- [6] H. Li, B. Manjunath, and S. K. Mitra, "Multisensor image fusion using the wavelet transform," *Graphical Models and Image Processing*, vol. 57, no. 3, pp. 235-245, May 1995.
- [7] A. L. Da Cunha, J. Zhou, and M. N. Do, "The nonsubsampled contourlet transform: theory, design, and applications," *IEEE Trans. on Image Processing*, vol. 15, no. 10, pp. 3089-3101, Oct. 2006.
- [8] W. W. Wang, P. L. Shui, and G. X. Song, "Multifocus image fusion in wavelet domain," in *Proc. Inter. Conf. Machine Learning and Cybernetics*, pp. 2887-2890, Xi'an, China, Nov. 2003.
- [9] N. Kingsbury, "Design of Q-shift complex wavelets for image processing using frequency domain energy minimization," in *Proc. Inter. Conf. Image Processing*, vol. 1, pp. 1013-1016, Barcelona, Spain, Sep. 2003.
- [10] J. L. Starck, J. Fadili, and F. Murtagh, "The Undecimated Wavelet Decomposition and its Reconstruction," *IEEE Trans. on Image Processing*, vol. 16, no. 2, pp. 297-309, Feb. 2007.
- [11] C. Chen, and C. Hsiao, "Haar wavelet method for solving lumped and distributed-parameter systems," *IEE Proc. on Control Theory and Applications*, vol. 144, no. 1, pp. 87-94, Jan. 1997.

- [12] W. Aili, Q. ChangYan, H. Yuhui, and L. Xusheng, "Multifocus image fusion based on nonsubsampling contourlet transform," in *Proc. 7th Inter. Forum Strategic Technology*, pp. 1-4, Tomsk, Russia, Sep. 2012.
- [13] J. Tian, L. Chen, L. Ma *et al.*, "Multi-focus image fusion using a bilateral gradient-based sharpness criterion," *Optics Communications*, vol. 284, no. 1, pp. 80-87, Jan. 2011.
- [14] K. Li, X. Chen, X. Hu, X. Shi, and L. Zhang, "Image denoising and contrast enhancement based on nonsubsampling contourlet transform," in *Proc. 3rd IEEE Inter. Conf. Computer Science and Information Technology*, pp. 131-135, Chengdu, China, Jul. 2010.
- [15] Y. Chai, H. Li, and X. Zhang, "Multifocus image fusion based on features contrast of multiscale products in nonsubsampling contourlet transform domain," *Optik-International Journal for Light and Electron Optics*, vol. 123, no. 7, pp. 569-581, Apr. 2012.
- [16] M. F. Yakhdani and A. Azizi, "Quality assessment of image fusion techniques for multisensor high resolution satellite images (case study: IRS-P5 and IRS-P6 satellite images)," in *Isprs TC VII symposium – 100 years ISPRS, IAPRS*, Vienna, Austria, Jul. 2010.
- [17] B. Yang, and S. Li, "Pixel-level image fusion with simultaneous orthogonal matching pursuit," *Information Fusion*, vol. 13, no. 1, pp. 10-19, Jan. 2012.
- [18] C. Xydeas, and V. Petrović, "Objective image fusion performance measure," *IET Electronics Letters*, vol. 36, no. 4, pp. 308-309, Feb. 2000.